PAPER

Crystallization of ZrO_2-nucleated $MgO/Al_2O_3/SiO_2$ glasses – a TEM study

Christian Patzig,*[a] Marc Dittmer,[b] Antje Gawronski,[b] Thomas Höche[a] and Christian Rüssel[b]

In a $61SiO_2\cdot17.5MgO\cdot17.5Al_2O_3\cdot4ZrO_2$ (mol%) glass, the course of crystallization at a heat treatment temperature of 950 °C is analyzed between $t = 0$ and 100 h using X-ray diffractometry and (scanning) transmission electron microscopy in combination with energy-dispersive X-ray spectroscopy at multiple stages of heat treatment. It is found that after an initial formation of phase-separation droplets from the vitreous parent glass, high-quartz solid solution crystals are formed, in which ZrO_2 nanocrystals are embedded. The diameters of the latter nanocrystals stay approximately constant at around 3.7 nm for all heat treatment times. In contrast to previous investigations of a SiO_2–MgO–Al_2O_3–ZrO_2 parent glass with slightly altered composition, no transformation from high- to low-quartz solid solution with increasing heat treatment time is observed here. Moreover, no precipitation of secondary phases like spinel or indialite occurs. Hypotheses concerning possible crystallization mechanisms that occur during heat treatment of the parent glass are discussed.

1 Introduction

In the absence of nucleating agents, glass-ceramics derived from $MgO/Al_2O_3/SiO_2$ parent glasses usually evolve due to surface crystallization upon heat treatment. The addition of nucleating agents such as TiO_2,[1–3] ZrO_2,[3–5] or a mixture of both,[6–8] however, may lead to bulk nucleation. For two reasons, this glass system has frequently been investigated. Without nucleating agents, it was studied with respect to its surface crystallization behaviour, mainly due to its potential applications as sintered glass-ceramics, *e.g.* for use as substrate material in electronics. The second reason is its pronounced mechanical strength, which can be achieved after supplying an appropriate heat treatment schedule to the parent glass. In the past few years, especially two potential applications were reported for glass-ceramics based on the system $MgO/Al_2O_3/SiO_2$: as substrate for hard discs[9] and as material for restorative dentistry.[10]

The high strength of the final glass-ceramic product is usually linked to the occurrence of α-quartz (that is, the low-temperature, hexagonal quartz modification) or α-quartz solid solution. It has been shown previously that the temporal evolution of volume crystallization in nucleated

$MgO/Al_2O_3/SiO_2$ glass-ceramics can proceed as follows:[4,11,12] during heat treatment, the nucleating agent is precipitated first. Triggered by the precipitation of these seed crystals, domains of a high-temperature quartz modification – β-quartz solid solution – that can accommodate, and, in fact, do incorporate large quantities of both MgO and Al_2O_3, are formed. Since the incorporation of MgO and Al_2O_3 in the β-quartz solid solution phase leads to a stabilisation thereof, the phase transition from β-quartz to α-quartz upon sample cooling, which – for pure quartz – usually occurs at a temperature of around 573 °C[12,13] (the temperature, however, will be different in this case since a transition from β- to α-quartz solid solution takes place here), may be hampered. This high-to-low-quartz (solid solution) transition, if occurring, is accompanied by a 0.8% volume contraction of the quartz domains. Furthermore, the thermal expansion coefficient $\alpha_{20\text{–}300\ °C} = 13.2 \times 10^{-6}\ K^{-1}$ (ref. 13) of the α-quartz (pure quartz, for α-quartz solid solution, different $\alpha_{20\text{–}300\ °C}$ values might occur) is much higher than that of the residual glass and hence leads to additional mechanical stresses during cooling. As such, contraction leads to high mechanical stresses in the formed crystals and in the surrounding glassy matrix. These, in turn, can result in high mechanical strengths of up to 450 MPa.[6,14] Furthermore, huge hardness values of up to 13 GPa and high Young's moduli of up to 140 GPa[1,8] can be obtained.

However, even if the high-to-low-quartz (solid solution) transition during sample cooling is hindered in the first place (due to a stabilisation of the β-quartz solid solution phase by means of MgO and Al_2O_3 incorporation therein), it

[a] Fraunhofer Institute for Mechanics of Materials IWM, Center for Applied Microstructure Diagnostics, Walter-Huelse-Straße 1, 06120 Halle (Saale), Germany. E-mail: Christian.Patzig@iwmh.fraunhofer.de; Fax: +49 345 5589 101; Tel: +49 345 5589 192

[b] Otto-Schott-Institut, Jena University, Fraunhoferstraße 6, 07743 Jena, Germany

can be induced if the β-quartz solid solution phase gets depleted from MgO and Al_2O_3 with on-going heat treatment, either due to higher temperatures or due to longer periods of heat treatment time.[4,11] This depletion runs parallel to a precipitation of crystalline phases that incorporate Mg, Al and O, like, for example, spinel ($MgAl_2O_4$).

The addition of at least 4 mol% of nucleating agents to an $MgO/Al_2O_3/SiO_2$ parent glass will promote the bulk uniform crystallization of a β-quartz (solid solution) phase.[15] For the $MgO/Al_2O_3/SiO_2$ glass system, ZrO_2 as well as TiO_2 are especially suitable as nucleating agents.[2–5] In previous studies, the phase formation and the resulting mechanical properties have intensely been described.[4,16] In the past, also effects of various additives such as P_2O_5,[14] CaO,[17] Y_2O_3,[15,16] and CeO_2 (ref. 9,18) on the crystallization behaviour and resulting mechanical properties of the glass-ceramics, were studied. It has also been shown that MgO can – at least partially – be replaced by ZnO,[8,19,20] without losing the good mechanical properties of the glass-ceramics.

Only few studies using transmission electron microscopy were carried out so far to investigate the microstructure and to give a structural explanation of the phase-formation process.[11,21] It should be emphasized again that phase formation and the microstructure depend much on the type and concentration of the used nucleating agents.

As recently reported, a heat treatment at a temperature of 950 °C of a $51.9SiO_2 \cdot 21.2MgO \cdot 21.2Al_2O_3 \cdot 5.7ZrO_2$ (mol%) glass, a system that in the following will be called "Z6" (due to its molar zirconia concentration), primarily leads to the formation of star-shaped zirconia crystals, and, after prolonged heat treatment, to the crystallization of the above-mentioned β-quartz solid solution crystals. In a final stage, Mg-, Al- and O-bearing spinel and indialite crystals are precipitated as well, thus increasing the likelihood of a high-to-low-quartz solid solution transition during sample cooling.[2,10,11,21]

It is shown in the following that the addition of a smaller ZrO_2 concentration (4 mol% instead of the aforementioned 5.7 mol%) to an MAS glass with altered composition leads to a drastic change in the entire phase formation process and, thus, in the resulting microstructure.

In this paper, the effect of a heat treatment at 950 °C on glasses with the molar composition $61SiO_2 \cdot 17.5MgO \cdot 17.5Al_2O_3 \cdot 4ZrO_2$ (mol%), a glass that will be referred to as "Z4" in the following, is studied with emphasis on the resulting microstructure. It could be presumed that the lower content of both MgO and Al_2O_3 in the glass Z4 with respect to the glass Z6 should be especially advantageous to enable the transformation of the high temperature phase β-quartz solid solution to the low temperature phase α-quartz (solid solution) easier, since the first-precipitated β-quartz solid solution phase should contain smaller quantities of MgO and Al_2O_3 than in the case of Z6. However, it will be shown in the following that fundamental differences concerning the crystallization process itself (including the absence of the high-to-low-quartz solid solution transition), as well as the resulting microstructure, arise between the systems Z4 and Z6.

2 Materials and methods

Glasses with the mol% composition $61SiO_2 \cdot 17.5MgO \cdot 17.5Al_2O_3 \cdot 4ZrO_2$ were melted from reagent grade raw materials SiO_2, $4MgCO_3 \cdot Mg(OH)_2 \cdot 5H_2O$, $Al(OH)_3$ and ZrO_2 in a platinum crucible. The melting temperature 1590 °C was kept for 2 h. The melt was cast into water, dried and crushed into glass pieces with particle diameters ≤1.25 mm. The glass was remelted at a temperature of 1590 °C, kept for another 2 h and subsequently cast on a copper block. It was placed in a muffle furnace, which previously was heated up to 830 °C, and then immediately slowly (around 2 K min⁻¹) cooled to room temperature.

Small pieces of glass were crystallized at a temperature of 950 °C for different periods of time (0–100 h) by supplying heating and cooling rates of 5 K min⁻¹.

After the heat treatment procedure, the investigation of crystal phases from the glass-ceramic samples was performed with X-ray-diffraction (XRD) of powdered samples (D5000 diffractometer, $Cu_{K\alpha}$ radiation [λ = 0.154 nm], Siemens Company) in a θ–2θ-setup in a 2θ range between 10° and 60°.

More detailed characterizations of the crystal phases and their surroundings were carried out using (scanning) transmission electron microscopy ([S]TEM) and energy-dispersive X-ray spectrometry (EDXS).

For TEM sample preparation, an all-mechanical, wedge-polishing route was chosen: using a specific tripod sample holder in combination with a multi-functional grinding and polishing tool (MultiPrep, Allied Company), a very thin, electron-beam transparent wedge was generated for each sample, by polishing them under a defined, very small angle (≈1.6°). Subsequently, for purposes of both cleaning and final thinning, the samples were ion-beam polished with low-energetic (≈2.5 keV) Ar⁺-ions (precision ion-polishing system PIPS, Gatan company) under grazing angle incidence (±5°). As the samples were non-conducting, area-selective carbon coating with a special coating mask[22] was carried out before TEM analyses.

The TEM analyses were performed on an FEI Titan³ 80–300 electron microscope (FEI Company) at 300 kV acceleration voltage. Using the same instrument, STEM employing a high-angle annular dark field (HAADF) detector (Fischione Model 3000, camera length: 145 mm) was accomplished. STEM in combination with EDXS (Super-X EDX detector, FEI Company) allowed to achieve distribution mappings of different elements of chosen samples, using the commercially available software Esprit (Bruker Company). Element distribution mappings were derived by evaluating the lateral distribution of the peak intensity, i.e., the area underlying the K_{α} edges (in case of Mg, Al, Si, O) or the L_{α} edge (in case of Zr) of the analyzed elements, with an automatic routine provided by the software. EDXS quantification was also done automatically by the software, evaluating the peaks of the K lines of the respective elements. Since a quantification of rather light elements, such as oxygen, is somewhat doubtful with EDXS, the oxygen K peak was only deconvoluted, but disregarded for quantification.

The evaluation of STEM micrographs in terms of the mean crystal diameter of the ZrO_2 precipitates in the samples was done using the software ImageJ (http://rsbweb.nih.gov/ij/). First, the micrographs were image processed in order to enhance the contrast of the ZrO_2 crystals. These appear bright in the STEM micrographs due to the fact that Zr is by far the heaviest element of the parent glass composition – since HAADF imaging in STEM is based on inelastic electron scattering due to interaction of the electron beam with sample atoms, and as the scattering cross section increases with higher atomic number Z of the atoms in the screened sample,[23] this Z-contrast imaging technique is ideally suited to detect Zr-rich sample regions.[11] Second, a Gaussian filter was applied for smoothing the micrographs, followed by eliminating the micrograph background. Third, a binarization of the processed micrographs was applied, and all ambiguous data (*e.g.*, several adjacent, separated crystals that are – incorrectly – detected as just one large crystal by the software) was carefully removed manually. Finally, the diameters of the as-detected crystals were automatically determined. In order to minimize non-systematic errors in this data evaluation scheme, care was taken to analyse all micrographs with the same routine and settings.

3 Brief conclusion of previously reported findings

As already described in section 1, we recently reported on the crystallization mechanism that is present in glasses Z6 with the composition $51.9SiO_2 \cdot 21.2MgO \cdot 21.2Al_2O_3 \cdot 5.7ZrO_2$ (mol%), when a heat treatment at a temperature of 950 °C is applied for different times t.[10,11,21]

In order to associate and classify the subsequently described results concerning the crystallization of the glass Z4 with the context of crystallization in Z6, a brief description of the latter can be described as follows:[11] without any observable phase-separation, crystallization starts with the nucleation of tiny, star-shaped ZrO_2 crystals. With ongoing heat-treatment, these ZrO_2 crystals increase in size, whilst they are surrounded by a zone that is, according to EDX results, depleted in Zr, as a consequence of the ZrO_2 growth. This compositional change of the vitreous matrix in close proximity to the star-shaped ZrO_2 crystals fosters the precipitation of β-quartz solid solution. With increasing heat treatment time, the β-quartz solid solution expands into the bulk sample volume, thereby expelling tiny, circular ZrO_2 crystals that subsequently get overgrown by and embedded in the β-quartz solid solution phase. After a certain heat treatment time, the expansion of β-quartz solid solution domains comes to an end in Z6, once the vast majority of the sample bulk is transformed from glassy to crystalline. During an ongoing heat treatment, the β-quartz solid solution domains will get depleted in MgO and Al_2O_3, since spinel and also indialite are precipitating at late stages of crystal growth, thereby soaking up Mg and Al. This depletion destabilizes the β-quartz solid solution domains against a transformation

to α-quartz solid solution upon sample cooling, which in fact takes place and can be monitored with XRD.

In the following, experimental results concerning the crystallization of the Z4 parent glass are given, and the results are compared with respect to the crystallization of the aforementioned parent glass Z6.

4 Results

XRD

Fig. 1 shows XRD patterns of samples of the parent glass Z4, heat treated at a temperature of 950 °C for different periods of time t.

According to XRD, the parent glass sample, as well as the samples heat treated for $t < 3$ h, show no indication for the precipitation of crystalline phases (in the XRD spectra only the sample of the parent glass and the sample heat treated for $t = 2$ h are shown from this t region).

In the sample heat treated for $t = 3$ h, a small peak at around 26° is observed, which is indicative of crystalline β-quartz solid solution, and can be attributed to the 100% peak thereof (JCPDS no. 11-0252). In the XRD patterns of the samples heat treated for longer times, this 100% peak of β-quartz solid solution, as well as further peaks that can be attributed to this phase, become visible. Additionally, peaks of minor intensity, which are attributable to zirconia (JCPDS no. 50-1089), can be discerned as well.

The inset in Fig. 1 depicts the 100% β-quartz solid solution peak in a higher magnification. This peak occurs at the same 2θ value for all heat treatment times applied. According to literature, a notable shift of this peak to values larger than 26° would indicate the existence of the hexagonal, low temperature α-quartz (solid solution) phase.[12] Since for all heat treatment times t the main quartz solid solution peak remains at the same position in the XRD patterns, it can be concluded that the high-to-low-quartz solid solution transition upon sample cooling does not occur for glass-ceramics obtained from the Z4 parent glass within the heat treatment scheme applied. This result is consistent with the finding
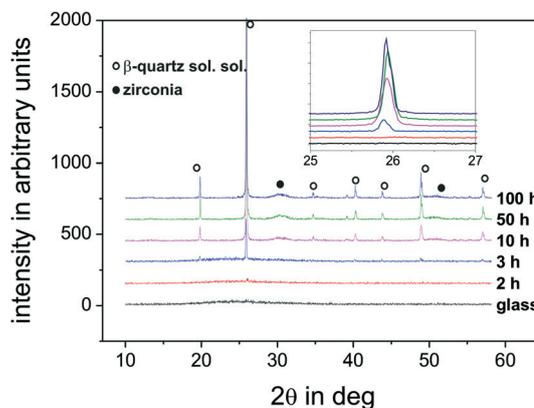
Fig. 1 XRD-patterns of the sample Z4, heat treated at 950 °C for different periods of time. Inset: magnified view of the main β-quartz solid solution peak at $2\theta \approx 26°$.

that peaks indicative of spinel (MgAl$_2$O$_4$, JCPDS no. 21-1152), or other crystalline oxides that host Mg and Al (*e.g.*, indialite or sapphirine) are not observed in the XRD patterns of Z4 after heat treatment at 950 °C for any time *t*. Furthermore, this finding is fundamentally different from the previously published results of the glass-ceramics obtained from parent glass Z6. In the Z6 samples, at the same temperature of 950° C, after *t* > 4 h spinel (and, later on, also indialite) precipitate, thus depleting the β-quartz solid solution from MgO and Al$_2$O$_3$, therefore enabling it to transform into α-quartz solid solution upon cooling.[11]

TEM/STEM and EDXS

In order to get a more detailed view on the temporal evolution of crystallization of the parent glass Z4 due to heat treatment at 950 °C, a detailed (S)TEM investigation including several samples, heat treated for various times *t*, was performed. In Fig. 2, a selection of STEM micrographs is shown that elucidates the microstructural change of the initially amorphous parent glass during temperature-induced volume crystallization: while after *t* = 0 h (temperature ramp-up only, Fig. 2(a)), the sample is still fully amorphous and homogeneous (on a mesoscopic length scale), the microstructure undergoes drastic changes with increasing heat-treatment time *t*. At *t* = 2 h (Fig. 2(b)), the sample is not homogeneous any more, but consists of a glassy matrix in which numerous phase-separation droplets are embedded. The diameter of these droplets is in the order of approximately 10 to 40 nm. Since HAADF imaging in STEM is basically a *Z*-contrasting technique, the less bright appearance of these droplets (compared to their surrounding matrix) already indicates that the droplet composition consists of lighter elements in relation to the parent glass composition. This is proven by EDXS element distribution mappings of a sample after *t* = 2 h (Fig. 3), that show that these phase-separation droplets are enriched in Si and also contain oxygen, but are depleted in all other elements of the parent glass composition. As such, this example shows that the EDXS mapping technique represents a valuable extension of the standard methods to visualise phase-separation structures in the TEM.[24] The finding that the phase-separation droplets are enriched in Si is different to other observations of the temporal course of crystallization in silicate glass-ceramics, where, if during the crystallization process a droplet phase is formed, this phase-separation structure is usually enriched in other elements, especially when these constitute an early crystalline phase in the final glass-ceramics. Examples are glass-ceramics from parent glasses consisting of SiO$_2$/Al$_2$O$_3$/Na$_2$O/LaF$_3$ in which the separation droplets are enriched in F, La, and Tm to form Tm^{3+} – doped LaF$_3$ in later stages of crystallization,[25] or multicomponent glass-ceramics from the lithiaaluminosilicate system in which phase-separation droplets occur that are enriched in zirconia, titania and alumina, and from which, in later stages of crystallization, ZrTiO$_4$ is precipitated, acting in due course as a nucleation agent.[26]
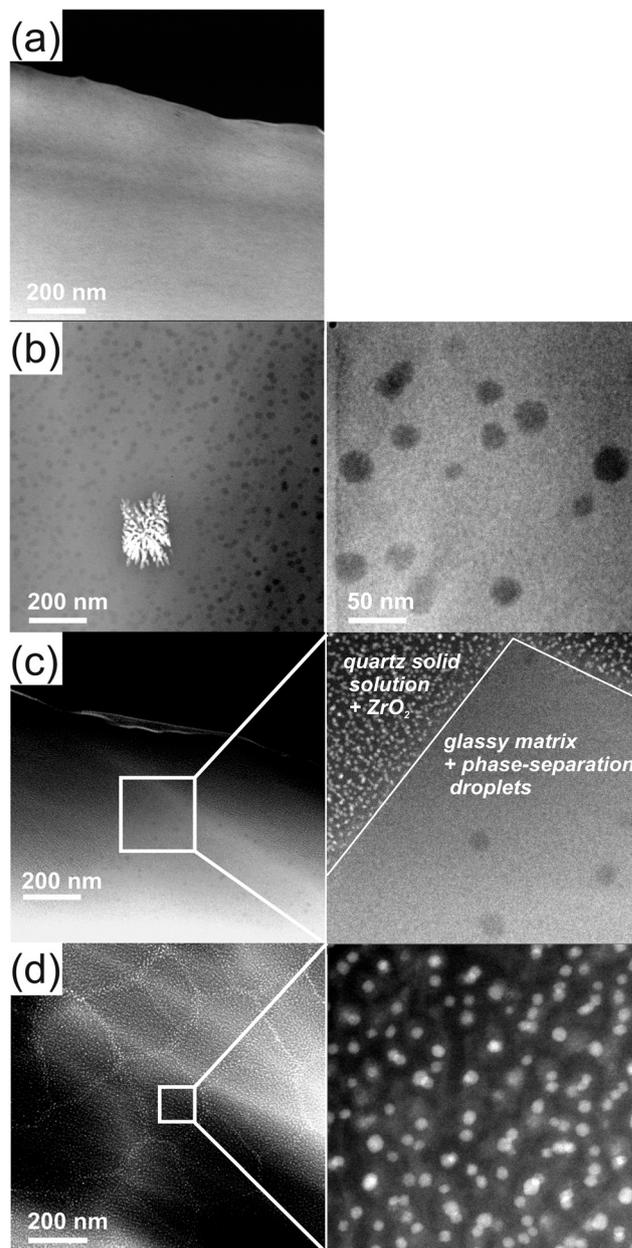

Fig. 2 STEM micrographs of glass-ceramics from the parent glass Z4, representing different heat treatment times *t*: (a) fully amorphous, homogenous sample after *t* = 0 h (temperature ramp-up only). (b) Left: liquid–liquid phase separation droplets after *t* = 2 h. Note the ZrO$_2$ dendrite co-existing with the droplets. Right: magnified view of glass matrix and phase separation droplets. (c) Co-existence of β-quartz solid solution domains with embedded ZrO$_2$ nanocrystals and domains that consist of glass matrix and phase separation droplets after *t* = 3 h. (d) Several β-quartz solid solution domains with embedded zirconia nanocrystals in fully crystallized sample after *t* = 10 h.

In the parent glass composition Z4 studied here, the addition of zirconia originally followed the idea of helping to foster volume crystallization by precipitating ZrO$_2$ in an early stage, in analogy to the previously studied system Z6. Instead, the formation of silica-rich droplets in the early stages of heat treatment seems (*cf.* Fig. 2(b), 3) to increase the
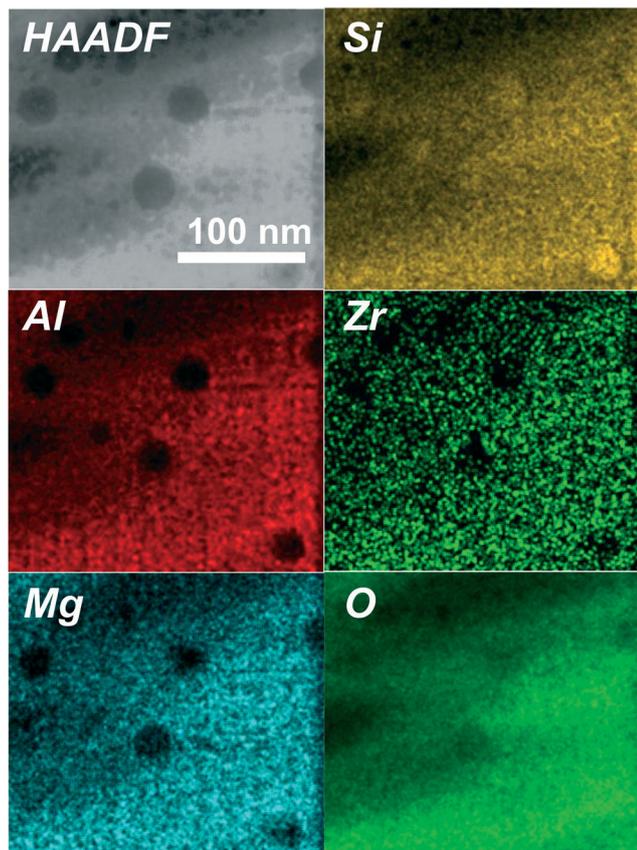
Fig. 3 STEM-EDXS mapping of the elements of parent glass Z4 after a heat treatment time of t = 2 h. The liquid–liquid phase separation droplets are enriched in Si and depleted in all other elements.

solubility of zirconia in the residual glass. Zr, Al, and Mg are not enriched in the droplet phase. Moreover, the crystallization behaviour is strikingly different from that of the parent glass composition Z6 that has previously been reported:[11] in Z6, no droplet phase is observed at all, but the crystallization starts with the precipitation of tiny, star-shaped ZrO_2 nuclei, that are present already after just ramping up the glass to 950 °C (t = 0 h). It is to be emphasized that the dendritic crystalline phase depicted in Fig. 2(b) which, according to XRD, consists of ZrO_2, is not directly comparable to the star-shaped ZrO_2 nuclei observed in Z6. While in Z6 the latter zirconia crystals clearly serve as nucleation agent for a subsequent precipitation of β-quartz solid solution,[11] the dendritic ZrO_2 crystals in the Z4 samples co-exist with the droplet phase (see Fig. 2(b)) and no obvious sign of β-quartz solid solution precipitation around them could be observed at any stage of heat treatment. Furthermore, the ZrO_2 dendrites that appear upon crystallization of the parent glass Z4 are larger and clearly of a different shape than the star-shaped ZrO_2 crystals that are present in Z6. Hence, it might well be that the cause for their appearance in Z4 is, for example, a local enrichment of zirconia due to local compositional inhomogeneities. The volume expansion of a β-quartz solid solution phase with a ZrO_2 dendrite as a nucleus, just as it appears upon heat treatment of the parent glass Z6, has, however, not

directly been observed with (S)TEM analyses during the temporal evolution of crystallization of the parent glass Z4. However, it cannot be excluded with certainty at this point that the dendritic ZrO_2 structures provoke β-quartz solid solution expansion, as will be discussed later.

For prolonged heat-treatment time, namely after t = 3 h, STEM microstructure analysis reveals the coexistence of two types of domains. While some part of the materials' volume is still occupied by the glassy phase that hosts phase-separated, Si-rich droplets, the other part consists of crystalline domains in which numerous, nanosized precipitates are embedded. The latter matrix phase appears darker in STEM micrographs than the vitreous matrix in which the phase-separation droplets are embedded (Fig. 2(c)). In parallel, the nanosized precipitates possess a rather high signal intensity in STEM micrographs. As discussed in the previous section, high intensities in STEM micrographs are indicative of Zr enrichments, since Zr is the heaviest element of the parent glass composition. According to that, the matrix surrounding the nanosized precipitates can be identified as the β-quartz solid solution phase, in which ZrO_2 nanocrystals are embedded. Different from that, the vitreous matrix that surrounds the phase-separated droplets in the other domains still contains zirconia. This is in agreement with XRD results (see Fig. 1), that prove the initial appearance of the β-quartz solid solution phase after t = 3 h.

Unfortunately, we have been unable to monitor the transition from the phase-separated droplet state to the β-quartz solid solution phase with embedded zirconia nanocrystals with (S)TEM in this study. Since it is impossible to monitor this transformation in situ, we had to rely on TEM samples that had undergone heat treatments for very specific times t, as such presenting "snapshots" of the crystallization process within the bulk of the samples. Neither could central nuclei (like the star-shaped ZrO_2 nuclei that initiate β-quartz solid solution crystallization in Z6 (ref. 11)) that are unambiguously surrounded by volume-expanding β-quartz solid solution be spotted, nor seems the phase-separated parent glass to hamper the spreading of the quartz solid solution domains. As such, the triggering structure or feature that precedes β-quartz crystallization in the glass Z4 is yet an open issue, as will be discussed later.

With increasing heat treatment time t, the amount and size of the β-quartz solid solution domains in the samples increases, until finally, after t = 10 h, the entire sample consists of β-quartz solid solution domains that incorporate ZrO_2 nanocrystals, as shown in Fig. 2(d). A complementary view on the nanostructure of a nanocrystal-bearing quartz solid solution domain is presented in Fig. 4, where the high-resolution TEM micrograph clearly illustrates the crystalline structure of the spherical ZrO_2 nanocrystals which are embedded in the quartz solid solution matrix. The lattice distance, that is highlighted in one of the nanocrystals in Fig. 4, is (within the error of measurement) approximately 0.295 ± 0.01 nm, being indicative of t-ZrO_2 (011)[27] or c-ZrO_2 (111).[28]

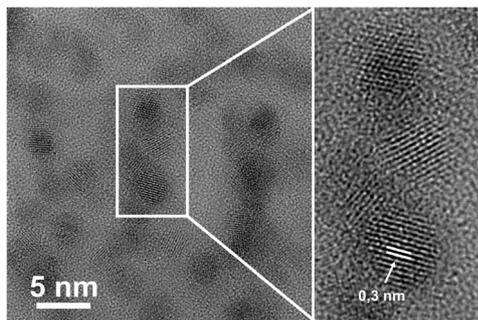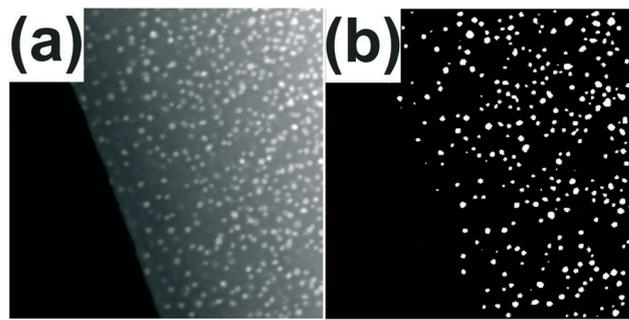As the STEM and XRD results indicate, the temporal evolution of crystallization of the glass Z4 upon heat treatment at

Fig. 4 High-resolution TEM micrograph of nanocrystalline ZrO_2 – bearing β-quartz solid solution domain of glass-ceramics from the parent glass system Z4 after t = 4 h. Left: magnified view of some ZrO_2 nanocrystals.

Fig. 5 (a) STEM micrograph of a glass-ceramic of parent glass Z4 after a heat treatment for t = 50 h. (b) Filtered and binarised image of the same micrograph for automated crystal detection, after careful removal of all ambiguous data. (c) Diameter class distribution of the detected crystals of the example shown in (a) and (b). (d) Relation of heat-treatment time t and mean ZrO_2 nanocrystal diameter for glass-ceramics of parent glass Z4.

950 °C is completed after a heat treatment time of $t \approx 10$ h. Most remarkably, a further increase of t does not at all alter the microstructure of the glass-ceramics, which is clearly different to the crystallization mechanism of the glass Z6, in which prolonged heat treatment led to the precipitation of spinel and indialite, as XRD[11] and STEM-EDXS[21] clearly proved, and to a subsequent high-to-low-quartz solid solution transition.
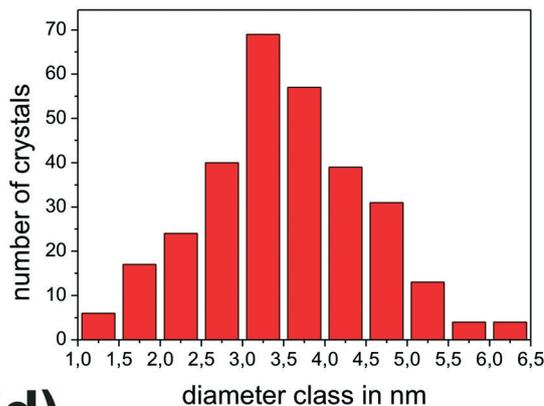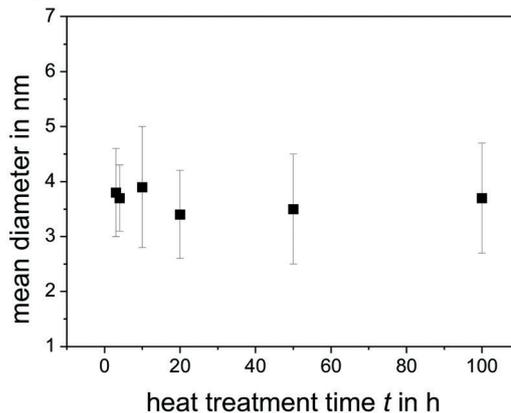
Besides (a) the absence of star-shaped ZrO_2 nuclei, (b) the presence of a phase-separated droplet stage during crystallization, and (c) the lacking precipitation of Mg- and Al-rich crystalline phases at late stages of crystallization, another important difference in the crystallization behaviour of the parent glass Z4 compared to that of Z6 consists in the diameter distribution of the spherical ZrO_2 nanocrystals. The mean diameter of the latter crystals (that are embedded in the quartz solid solution domains) remains strikingly constant for all heat treatment times: the evaluation of STEM micrographs of samples that were heat treated for times t between 3 h and 100 h reveals that the diameter distribution in each of the samples is rather narrow, see Fig. 5. Derived from Gaussian fits to the respective size-distribution curves, mean diameters are plotted against the heat-treatment time in Fig. 5(d). As can be seen there, these mean diameters stay constant at (3.7 ± 0.8) nm over a wide range of heat treatment times. On the contrary, in glass-ceramics obtained from the parent glass Z6, the mean diameter of these secondary ZrO_2 precipitations ranges between 5 and 10 nm.[11]

5 Discussion

In the previously studied parent glass Z6, precipitation of ZrO_2 nanocrystals within the expanding β-quartz solution domains most likely results from an expulsion of zirconia.[11] Being unable to accommodate zirconia beyond a certain solubility limit, the concentrically growing β-quartz solid solution domains push Zr ahead of the crystallization front. For thermodynamic reasons and in close 3D analogy of the 2D phenomenon of the Rayleigh instability (being responsible for the transformation of nanowires into a chain of nanodots[29]), instead of forming concentric, closed shells of

ZrO_2 around the β-quartz solid solution crystals, concentric shells of zirconia nanocrystals are formed. This evolution starts at the initial, star-shaped ZrO_2 nuclei.[11]

In the Z4 glass studied here, no star-shaped ZrO_2 nuclei were found during any stage of the heat treatment. By contrast, larger, dendritic ZrO_2 structures were observed, that already co-exist with the Si-rich droplets during the phase-separation stage of heat treatment, as can be seen in

Fig. 2(b). Other than for the glass-ceramics derived from the Z6 glass, however, these dendrites could not unambiguously be identified as trigger for the sudden precipitation of the β-quartz solid solution domains after $t \approx 3$ h.

Thus, various different crystallization mechanisms that can lead to the final glass-ceramics which consist of quartz solid solution domains – with embedded ZrO_2 nanocrystals that have a very narrow diameter distribution – are imaginable, which will be discussed in the following. A sketch of these three possible nucleation mechanisms is shown in Fig. 7, depicting the crystallization route with increasing heat treatment time, from the Z4 parent glass, over the phase-separated state to the final Z4 glass-ceramics.

The first (and probably most plausible) possible crystallization mechanism of the glass-ceramics in the system Z4 would directly be comparable to that of Z6, if it is assumed that the rather large, dendritic ZrO_2 crystals that already exist in the samples during the phase-separated stage (as shown in Fig. 2(b)) act as nucleation agents for the quartz solid solution expansion, just as the star-shaped ZrO_2 nuclei do in the system Z6 at a heat treatment at 950 °C.[11] In the samples derived from glass Z6, it was clearly visible that the crystallization of the β-quartz solid solution directly starts upon a Zr-depleted zone that surrounds the star-shaped ZrO_2 nuclei. By contrast, we were unable to monitor such an expansion of a crystal phase in direct vicinity of the dendritic ZrO_2 crystals in Z4. Thus, unlike for Z6, no direct proof of this hypothesis can be given here. It should, however, be mentioned that during phase-separation which occurs in the system Z4 in the early stages of temperature treatment, the glassy matrix itself, containing Si-rich droplets, has an initial composition that consists of less Si than the original base glass. Hence, this composition will be closer to that of Z6, and therefore, the crystallization of the β-quartz solid solution might be similar to that of Z6 as described previously,[11] with ZrO_2 dendrites in Z4 that replace the star-shaped ZrO_2 crystals from Z6 as nucleation agents for the β-quartz solid solution. Indeed, quantitative EDXS results taken from areas of the size $\approx 150 \times 150$ nm^2 from the glassy matrix, afar from the Si-rich droplets, of the sample after $t = 2$ h indicated a composition "in-between" Z4 and Z6 there: in the Z4 base glass, the molar cation ratio of Mg : Al : Si : Zr should be approximately 15 : 30 : 52 : 3 (atom%). In the Z6 base glass, it should be approximately 17 : 35 : 43 : 5 (atom%). In the remaining glassy matrix areas during the phase-separated state after $t = 2$ h in the system Z4, however, it was, according to EDXS, found to be approximately 17 : 32 : 47 : 4 (in atom%), which is somewhat closer to the Z6 base glass than to the Z4 base glass, indicating that the crystallization mechanism of this glassy matrix might be comparable to that of Z6.

However, as has already been stated before, an expanding, yet still small β-quartz solid solution domain that unambiguously circumscribes a dendritic ZrO_2 crystal, in analogy to the volume expansion of β-quartz solid solution around the star-shaped ZrO_2 crystals in the system Z6, could not be observed in Z4 during the phase-separated state.

A second possible crystallization trigger might as well be constituted by the Si-rich phase-separation droplets that form in the early stages of heat treatment. Due to the diffusion processes that must occur in order to generate these droplets, the distribution of elements, that is supposed to be homogeneous in the parent glass, changes. Since in the proximity of the Si-rich droplets that are embedded in the glassy matrix, the composition of the latter is most likely different from matrix areas that are further away from the droplet, this composition gradient in the diffusion zone around the Si-rich droplets could as well be a driving force for a subsequent β-quartz solid solution crystallization. In this scenario, the nanocrystalline, spherical ZrO_2 precipitations would again be a result of a Zr expulsion of the afore-expanding β-quartz solid solution crystal.

During crystallization of the glass Z6, the precipitation of the small, spherical ZrO_2 nanocrystals within the β-quartz solid solution domain is a consequence of the crystallization
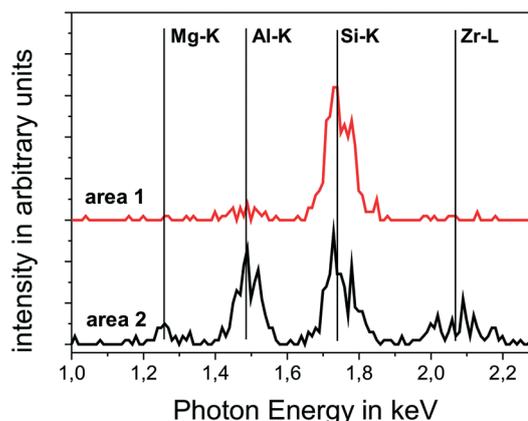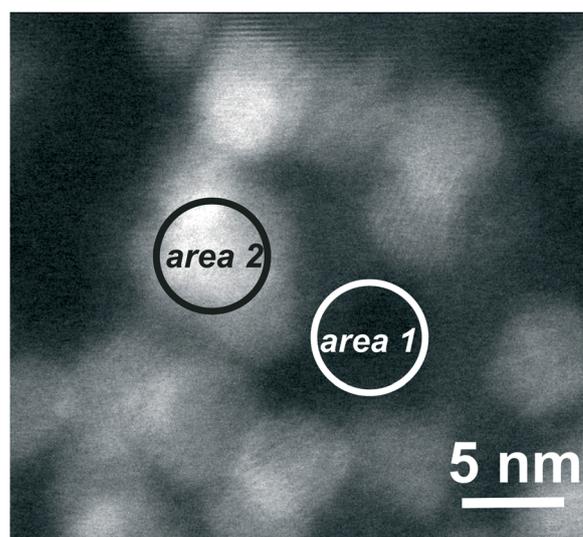

Fig. 6 STEM micrograph and area-selective EDX spectra of ZrO_2 nanocrystals in the β-quartz solid solution matrix in glass-ceramics of parent glass Z4 after $t = 10$ h heat treatment time. The spectral positions of the Mg–K, Al–K, Si–K, and Zr–L peaks are indicated in the spectra.

of the quartz itself.[11] Different from that, as a third possible crystallization mechanism for glass Z4, one might assume that there, not the β-quartz solid solution crystallizes first, but the spherical ZrO_2 nanocrystals. Upon formation of the phase-separated droplet phase, the enrichment of Si in the droplets will lead to a local increase of the Zr concentration in the droplet-surrounding matrix. This might induce a spontaneous precipitation of the ZrO_2 nanocrystals therein, which in turn might serve as nuclei for the crystallization of the ZrO_2-surrounding β-quartz solid solution phase. It was shown previously that during nucleation of the parent glass Z6, directly around the star-shaped ZrO_2 precipitates that serve as nuclei for the expansion of the crystalline β-quartz solid solution phase, a Zr-depleted zone forms in the vitreous matrix around these nuclei, and it was argued that this local change of the chemical composition might offer ideal conditions for β-quartz solid solution precipitation.[11,21] In the case of Z4, as the area-selective EDXS results indicate in Fig. 6, the local chemical environment might well be different in close proximity to the ZrO_2 nanocrystals in comparison with the surrounding β-quartz solid solution matrix. An Al and also Mg enrichment can be found in the area of the sample that incorporates a ZrO_2 nanocrystal, whereas in the β-quartz solid solution matrix area next to it, mainly Si contributes to

the EDX spectrum. These indications lead to the assumption that an Al- and possibly also Mg-enriched shell circumscribes the ZrO_2 nanocrystals, even at late stages of crystallization in which these nanocrystals are already embedded in the β-quartz solid solution. Assuming that (few) ZrO_2 crystals precipitate prior to the β-quartz solid solution formation, the existence of an Al- and Mg-rich shell around them would imply that locally, the composition of the glassy matrix would be changed. This chemical inhomogeneity in turn might trigger the β-quartz solid solution crystallization, just as it is the case in the glass Z6 due to a local depletion in Zr around the star-shaped ZrO_2 nuclei there. The possible existence of such a shell would also explain the constant, small diameter of approximately 3.7 nm that the ZrO_2 nanocrystals possess independently of the heat treatment time, since it would inhibit further diffusion of Zr from the vitreous matrix towards the nanocrystal. Highly viscous layers that act as diffusion barriers and suppress further growth of nanocrystals that precipitate from glassy matrices have been reported to exist during crystallization of several parent glass systems, including $Na_2O/K_2O/CaO/CaF_2/Al_2O_3/SiO_2$ glasses from which the precipitation of CaF_2 nanocrystals during heat treatment is reported,[30] as well as multicomponent lithium aluminosilicate glasses in which the existence of an alumina shell
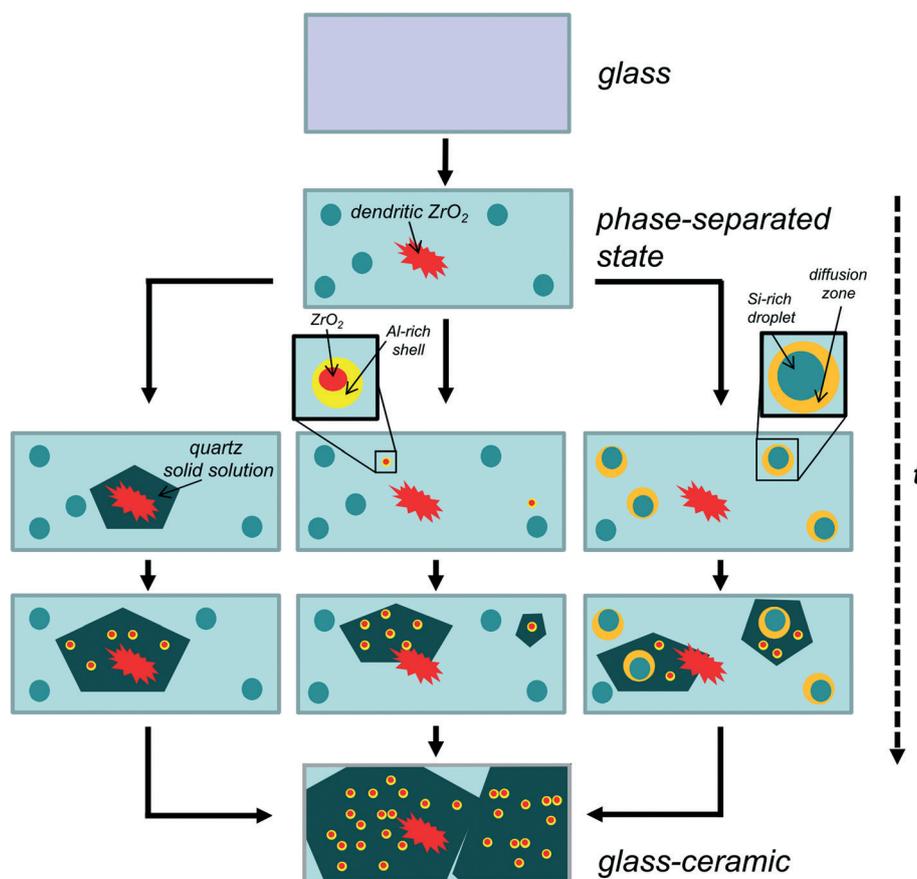

Fig. 7 Sketch to illustrate the proposed three different crystallization mechanisms with ongoing heat treatment time *t*. The left part of the illustration is a depiction of the first, the right part of the second, and the middle part of the third possible crystallization route that is hypothesized in the text.

around $ZrTiO_4$ nanocrystals upon crystallization was shown,[26] or $SiO_2/Al_2O_3/Na_2O/K_2O/BaF_2$ glasses, in which a silica shell forms around BaF_2 crystals during temperature-induced crystallization.[31] However, a more or less simultaneous nucleation of the nanosized, spherical ZrO_2 precipitations, followed by β-quartz solid solution crystallization, seems implausible to a certain degree, since at an intermediate stage of the heat treatment, already crystallized β-quartz solid solution domains co-exist with vitreous domains that consist of the phase-separated glassy phase, in which no signs of ZrO_2 nanocrystals are found (*cf.* Fig. 2(c)). It seems unreasonable that a nucleation of a large quantity of nanosized ZrO_2 precipitations should start in one part of the sample that has a well-defined border to another sample part in which no ZrO_2 nanocrystals at all are visible. However, if a precipitation of ZrO_2 nanocrystals that are encased by an Al-rich shell is assumed to be the starting point for a subsequent β-quartz solid solution precipitation, one might argue that only a few ZrO_2 nanocrystals precipitate in a first place, upon which the β-quartz solid solution starts to expand into the sample volume, thereby continuously expelling ZrO_2 that remains in nanocrystalline form, in a crystallization mechanism comparable to that of the system Z6.[11] If this is the case, then the vast majority of the ZrO_2 nanocrystals that are embedded in the β-quartz solid solution domains did not exist prior to the β-quartz solid solution phase, only very few ZrO_2 nanocrystals would then play the role of triggering the β-quartz solid solution nucleation. This would, however, also imply that Zr, Al, and Mg are locally enriched on the nanoscale already in the glassy phase, since otherwise it would not be plausible why the Al and Mg content should be enhanced close to the ZrO_2 nanocrystals that get expelled by a continuously growing β-quartz solid solution domain. Additionally, it has to be mentioned that if this third crystallization mechanism is at work, the co-existence of the large, dendritic ZrO_2 dendrites can not be denied, and it seems unplausible to a certain degree why spontaneously nucleated, spherical nanocrystals should foster a following β-quartz solid solution expansion, whereas the larger, dendritic ZrO_2 crystals do not act in the same way. Thus, if the third hypothesized nucleation mechanism should be at work at all, it is likely that it is co-existing with the first suggested mechanism.

6 Conclusions

In this study, the crystallization behaviour upon heat treatment at 950 °C for several times of Z4 glass ceramics with the composition $61SiO_2 \cdot 17.5MgO \cdot 17.5Al_2O_3 \cdot 4ZrO_2$ (mol%) was analyzed and compared to that of Z6 glass ceramics with a composition of $51.9SiO_2 \cdot 21.2MgO \cdot 21.2Al_2O_3 \cdot 5.7ZrO_2$ (mol%), which was previously described.[11] From both glasses, quartz solid solution and ZrO_2 are precipitated. Nevertheless, it was observed that very distinct differences occur between Z4 and Z6, concerning both the crystallization route at intermediate heat-treatment times and the phase content of the final glass-ceramics. Unlike in Z6, an early

phase-separated stage occurs during crystallization of Z4. Furthermore, no transformation from high- to low-quartz solid solution can be observed in Z4, even after prolonged heat-treatment times, which goes in hand with the non-appearance of Mg- and Al-bearing crystalline phases like spinel or indialite, that are both precipitated in Z6 after sufficiently long heat treatment.

Since it was not possible to monitor the transition from the phase-separated state to the precipitation of β-quartz solid solution and ZrO_2 in Z4 in the scope of this TEM study, several suppositions were made concerning the possible crystallization mechanisms during heat treatment of the Z4 glass, and three different, possible crystallization routes from parent glass to glass-ceramic were depicted. It is assumed that a local change of the glass composition is at work during the heat treatment of Z4, which presumably offers ideal conditions of a β-quartz solid solution precipitation there. This local composition change might be found either in the vicinity of small ZrO_2 nuclei, or around larger ZrO_2 dendrites, or, as a last possibility, surrounding Si-rich droplets in the phase-separated phase.

Although no definite picture of the temperature-induced crystallization of glasses from the composition Z4 could be drawn in this study, the tremendous differences that occur during crystallization of glasses from the system $MgO/Al_2O_3/SiO_2/ZrO_2$ due to a change of the base glass composition and amount of nucleating agent are yet another example of the diversity of both the acting crystallization processes[32] and, subsequently, the occurring crystalline phases in the final glass-ceramics that might be encountered when dealing with the crystallization of multi-component glasses.

Acknowledgements

References

1   P. Wange, T. Höche, C. Rüssel and E. D. Schnapp, *J. Non-Cryst. Solids*, 2002, **298**, 137–145.
2   W. Zdaniewski, *J. Mater. Sci.*, 1973, **8**, 192–202.
3   W. Zdaniewski, *J. Am. Ceram. Soc.*, 1975, **58**, 163–169.
4   M. Dittmer, M. Müller and C. Rüssel, *Mater. Chem. Phys.*, 2010, **124**, 1083–1088.
5   M. McCoy, W. E. Lee and A. H. Heuer, *J. Am. Ceram. Soc.*, 1986, **69**, 292–296.
6   A. Hunger, G. Carl, A. Gebhardt and C. Rüssel, *J. Non-Cryst. Solids*, 2008, **354**, 5402–5407.
7   A. Hunger, G. Carl, A. Gebhardt and C. Russel, *Mater. Chem. Phys.*, 2010, **122**, 502–506.
8   A. Hunger, G. Carl and C. Rüssel, *Solid State Sci.*, 2010, **12**, 1570–1574.

9 S. B. Sohn, S. Y. Choi and Y. K. Lee, *J. Mater. Sci.*, 2000, **35**, 4815–4821.

10 M. Dittmer and C. Rüssel, *J. Biomed. Mater. Res., Part B*, 2012, **100**, 463–470.

11 C. Patzig, M. Dittmer, T. Höche and C. Rüssel, *Cryst. Growth Des.*, 2012, **12**, 2059–2067.

12 A. Petzold and W. Hinz, *Silikatchemie*, VEB Verlag, Leipzig, 1978.

13 W. Vogel, *Glass Chemistry*, Springer, Berlin/Heidelberg, 1994.

14 A. Katzschmann and P. Wange, *Glass Sci. Technol. (Offenbach, Ger.)*, 1995, **68**, 111–116.

15 M. Dittmer, C. F. Yamamoto, C. Bocker and C. Rüssel, *Solid State Sci.*, 2011, **13**, 2146–2153.

16 A. Gawronski and C. Rüssel, *J. Mater. Sci.*, 2013, **48**, 3461–3468.

17 G. H. Chen, *J. Mater. Sci.*, 2007, **42**, 7239–7244.

18 S. B. Sohn and S. Y. Choi, *J. Non-Cryst. Solids*, 2001, **282**, 221–227.

19 L. R. Pinckney and G. H. Beall, *J. Non-Cryst. Solids*, 1997, **219**, 219–227.

20 G. H. Chen and X. Y. Liu, *J. Alloys Compd.*, 2007, **431**, 282–286.

21 C. Patzig, T. Höche, Y. F. Hu, H. Ikeno, M. Krause, M. Dittmer, A. Gawronski, C. Rüssel, I. Tanaka and G. H. Henderson, *J. Non-Cryst. Solids*, 2014, **384**, 47–54.

22 T. Höche, J. W. Gerlach and T. Petsch, *Ultramicroscopy*, 2006, **106**, 981–985.

23 Z. W. Wang, Z. Y. Li, S. J. Park, A. Abdela, D. Tang and R. E. Palmer, *Phys. Rev. B: Condens. Matter Mater. Phys.*, 2011, **84**, 073408.

24 S. Bhattacharyya, T. Höche, K. Hahn and P. A. van Aken, *J. Non-Cryst. Solids*, 2009, **355**, 393–396.

25 A. de Pablos-Martin, C. Patzig, T. Höche, A. Duran and M. J. Pascual, *CrystEngComm*, 2013, **15**, 6979–6985.

26 S. Bhattacharyya, T. Höche, J. R. Jinschek, I. Avramov, R. Wurth, M. Müller and C. Rüssel, *Cryst. Growth Des.*, 2010, **10**, 379–385.

27 J. Malek, L. Benes and T. Mitsuhashi, *Powder Diffr.*, 1997, **12**, 96–98.

28 D. N. Wang, Y. Q. Guo, K. M. Liang and K. Tao, *Sci. China, Ser. A: Math., Phys., Astron.*, 1999, **42**, 80–86.

29 M. E. Toimil-Molares, L. Rontzsch, W. Sigle, K. H. Heinig, C. Trautmann and R. Neumann, *Adv. Funct. Mater.*, 2012, **22**, 695–701.

30 C. Rüssel, *Chem. Mater.*, 2005, **17**, 5843–5847.

31 S. Bhattacharyya, C. Bocker, T. Heil, J. R. Jinschek, T. Höche, C. Rüssel and H. Kohl, *Nano Lett.*, 2009, **9**, 2493–2496.

32 T. Höche, *J. Mater. Sci.*, 2010, **45**, 3683–3696.